Distribution of directional change as a signature of complex dynamics

Stanislav Burov[a], S. M. Ali Tabei[a], Toan Huynh[b], Michael P. Murrell[c], Louis H. Philipson[d], Stuart A. Rice[a,b,1], Margaret L. Gardel[a,c,e], Norbert F. Scherer[a,b,c], and Aaron R. Dinner[a,b,c,1]

[a]James Franck Institute, [b]Department of Chemistry, [c]Institute for Biophysical Dynamics, [d]Department of Medicine, and [e]Department of Physics, University of Chicago, Chicago, IL 60637

Contributed by Stuart A. Rice, October 18, 2013 (sent for review July 30, 2013)

Analyses of random walks traditionally use the mean square displacement (MSD) as an order parameter characterizing dynamics. We show that the distribution of relative angles of motion between successive time intervals of random walks in two or more dimensions provides information about stochastic processes beyond the MSD. We illustrate the behavior of this measure for common models and apply it to experimental particle tracking data. For a colloidal system, the distribution of relative angles reports sensitively on caging as the density varies. For transport mediated by molecular motors on filament networks in vitro and in vivo, we discover self-similar properties that cannot be described by existing models and discuss possible scenarios that can lead to the elucidated statistical features.

random walks | angular correlation | cytoskeleton

Complex dynamics often emerge from ensembles of interacting constituents. Trajectories that are obtained by tracking individual constituents contain information beyond the evolution of ensemble properties, and these data can thus reveal new mechanistic features of the system studied. Examples cut across disciplines and include quantum dots (1), colloidal beads (2), features in cells (3, 4), fish in schools (5), birds in flocks (6), and primates in social groups (7, 8). These data (individual trajectories) demand theoretical frameworks for characterizing and interpreting them.

The standard reporter for different forms of motion is the mean square displacement (MSD)

$$\left\langle \overline{\mathbf{R}^2(T,\Delta)} \right\rangle = \frac{1}{T-\Delta}\int_0^{T-\Delta} \left|\mathbf{X}(t+\Delta)-\mathbf{X}(t)\right|^2 dt, \qquad [1]$$

where brackets and overlines denote ensemble and time averages, respectively. In simple Brownian motion (9), the MSD grows linearly with the separation in time between two observation points (the lag time, Δ) and does not depend on the amount of data included in averages (the measurement time, T)—i.e., there is ergodicity. Anomalous (i.e., non-Brownian) dynamics can arise from correlations in the walk steps. Correlations in the step sizes [e.g., as in fractional Brownian motion (FBM)] (10) give rise to nonlinear scaling of the MSD with lag time, retaining ergodicity (11). By contrast, a power-law distribution of dwell times [e.g., as in a continuous time random walk (CTRW)] (12) is associated with linear scaling with lag time but nonergodicity (13, 14). The two types of correlations can exist together (4, 15).

Despite the success of the MSD as an order parameter for dynamics, it is essentially a 1D measure. We expect random walks in two and more dimensions to contain information beyond the MSD, and various alternative analyses have been suggested (16) (*Conclusions*). In this paper, we introduce a statistical measure of such information. Specifically, we consider the relative angle, which quantifies the direction of motion over successive time intervals. We show that different models of stochastic processes give rise to different distributions of relative angles and how the intervals can be varied to probe contributing time scales. We apply our order parameter to 2D experimental data obtained for mesoscopic systems. We examine colloidal suspensions at two densities and show that the distribution of relative angles is a sensitive means of detecting and quantifying caging. Two different cytoskeletal systems are considered: insulin-containing vesicles (granules) in a pancreatic cell line (4) and in vitro mixtures of purified myosin motors and actin filaments. These active systems exhibit a common signature of directional motion that cannot be understood in terms of existing models. We propose possible scenarios that could lead to the observed statistics. Together, these examples show that the distribution of relative angles is a straightforward probe of complex dynamics that provides information beyond the MSD.

Construction of the Relative Angle

In this section, we introduce our order parameter for quantifying directional change. As shown in Fig. 1, each trajectory comprises a set of recorded positions of the particles $\mathbf{X}(t)$. Given these data, we form the vectors that connect positions separated by Δ steps, $\mathbf{V}(t;\Delta)=\mathbf{X}(t+\Delta)-\mathbf{X}(t)$. We define the relative angle $\theta(t;\Delta)$ as the angle between $\mathbf{V}(t;\Delta)$ and $\mathbf{V}(t+\Delta;\Delta)$

$$\cos\theta(t;\Delta)=\frac{\mathbf{V}(t;\Delta)\cdot\mathbf{V}(t+\Delta;\Delta)}{|\mathbf{V}(t;\Delta)||\mathbf{V}(t+\Delta;\Delta)|}. \qquad [2]$$

In analogy to Eq. **1**, the parameter Δ plays the role of a lag time; it controls the degree of temporal coarse-graining. For a given Δ, we compute $\theta(t,\Delta)$ across all times in each trajectory and then across all particles. We build a histogram of these values and normalize such that it integrates to one. The resulting probability density function, $P(\theta;\Delta)$, serves as our order parameter. We repeat this procedure for different Δ and examine how the order parameter changes. The quantity that we calculate, Eq. **2**, is reminiscent

Significance

Since Einstein's seminal work in 1905, the main means of characterizing stochastic processes has been the mean square displacement (MSD). However, this order parameter fails to capture many features of dynamics at the forefront of science today, ranging from glassy relaxation to active transport in biological cells. Although there have been several studies seeking to go beyond the MSD, such studies have not made full use of the information available in individual trajectories in two (or more) dimensions, as are now commonly obtained in particle tracking experiments. Here, we introduce an approach that quantifies directional properties of complex motions and discover striking correlations in a number of condensed phase systems.

Author contributions: S.B., S.M.A.T., S.A.R., N.F.S., and A.R.D. designed research; S.B., S.M.A.T., T.H., and M.P.M. performed research; L.H.P. and M.L.G. contributed new reagents/analytic tools; and S.B., N.F.S., and A.R.D. wrote the paper.

The authors declare no conflict of interest.

[1]To whom correspondence may be addressed: E-mail: s-rice@uchicago.edu or dinner@uchicago.edu.

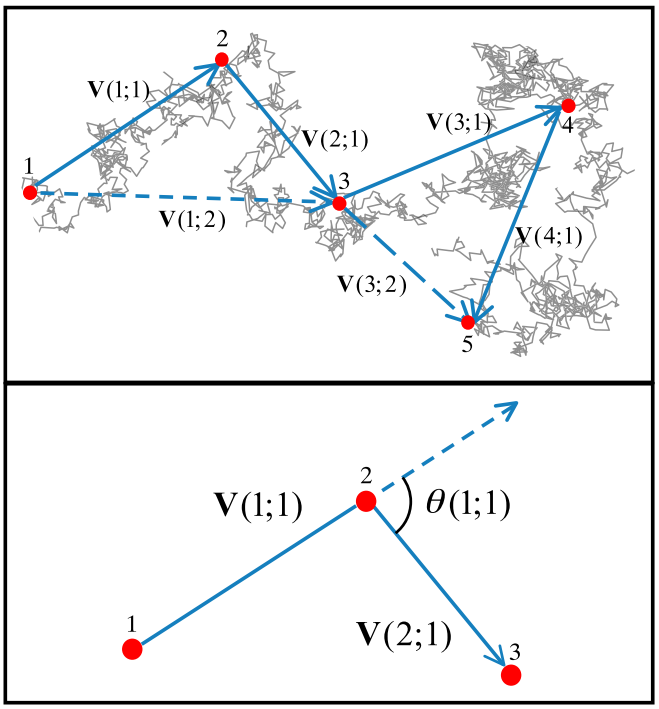

Fig. 1. Schematic of the construction of relative angles. (*Upper*) We sample a Brownian motion (gray line) at regular time intervals (red circles); these points are connected by vectors and angles between successive vectors are calculated. One time interval ($\Delta = 1$) is indicated by the solid blue arrows, and another, which is twice as long ($\Delta = 2$), is indicated by the dashed blue arrows. (*Lower*) Calculation of the angle $\theta(1;1)$ given the vectors in the first two (shorter) time intervals in the upper panel.

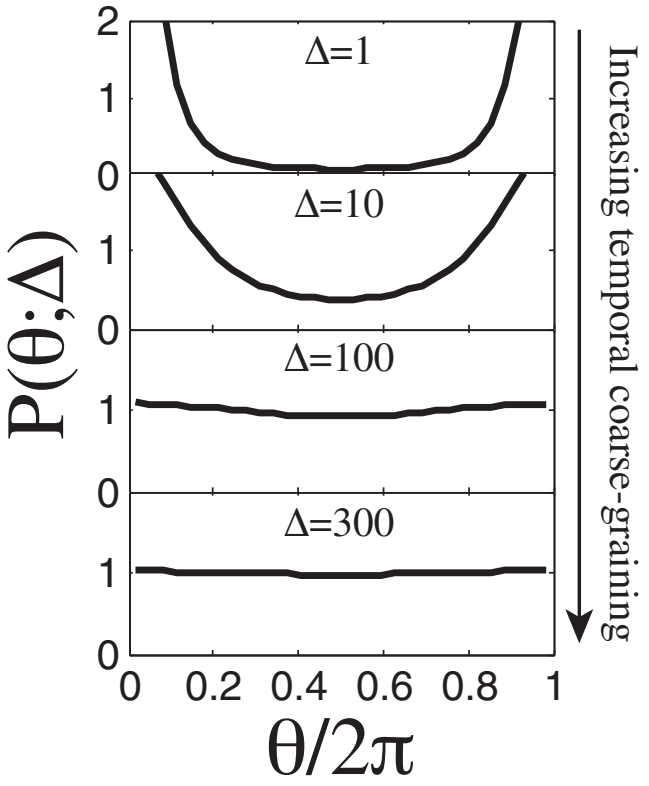

Fig. 2. Relative angle distributions for underdamped motion with various degrees of temporal coarse-graining (see text). Histograms are for a trajectory of 10,000 steps generated by leapfrog integration (35) of Eq. **3** with time step 0.1 with $\gamma/m = 1$ and $\sqrt{\mathcal{D}}/m = 1$; the sampling interval (unit of $\mathcal{D}$) is one time step.

of a velocity autocorrelation function (17), but it differs in that the **V** vectors are not instantaneous velocities and, importantly, we do not ensemble average.

Dictionary of Model Signatures

The variation in $P(\theta;\Delta)$ with Δ can serve as a signature of different types of motion. As a simple example, consider an inertial Langevin dynamics (17)

$$m\frac{d^2\mathbf{X}}{dt^2} = -\gamma\frac{d\mathbf{X}}{dt} + \boldsymbol{\xi}(t). \qquad [3]$$

Here m is the mass of the particle, $-\gamma d\mathbf{X}/dt$ is a drag, and $\boldsymbol{\xi}(t)$ is a 2D noise vector $(\xi_x(t), \xi_y(t))$ where $\xi_x(t)$ and $\xi_y(t)$ are Gaussian distributed uncorrelated noises $\langle\xi_y(t)\xi_x(t')\rangle = \mathcal{D}\delta_{xy}\delta(t-t')$, where $\delta(t-t')$ is the Dirac δ-function, δ_{xy} is the Kronecker δ-function, and $\mathcal{D}$ is a constant noise strength (the brackets indicate ensemble averaging). We integrate this equation of motion to obtain a 2D trajectory. When $\Delta = 1$ (Fig. 2, *Upper*), the distribution is peaked at $\theta = 0$, which is equivalent to $\theta = 2\pi$ owing to the periodicity of the angle. The U-shape in this representation is a signature of inertial motion: at short times the particle tends to continue in the same direction. As Δ increases, the noise randomly shifts the direction of travel, causing the distribution to flatten steadily (Fig. 2, lower three panels). For sufficiently large temporal coarse-graining, successive vectors between sampled points $[\mathbf{V}(t;\Delta)]$ are completely independent and the distribution is that of a simple random walk (Fig. 2, Δ = 300). The distribution remains flat for all further times, a signature of the self-similarity of diffusion (18).

We can similarly understand the signatures of motions that are influenced by various potentials. In Fig. 3*A*, we show $P(\theta;\Delta)$ for various Δ for diffusion of a particle in a box. At short times, the particle does not feel the boundary and the motion is just a simple random walk. As the temporal coarse-graining increases, a peak grows at $\theta = \pi$. This peak indicates that the successive vectors between sampled points are anticorrelated in direction—the reflecting boundaries force the particle to reverse its motion. Eventually

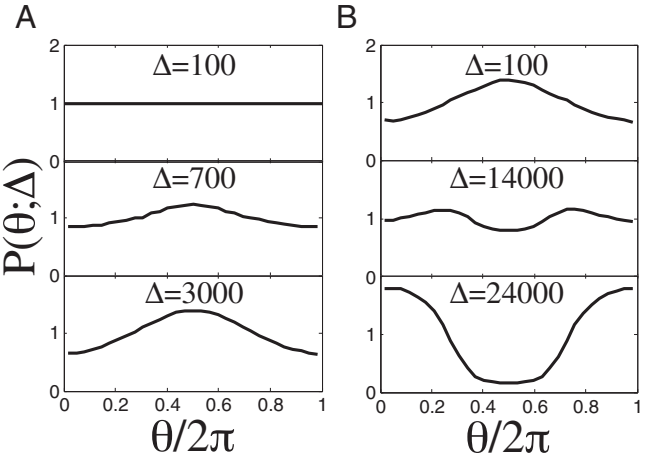

Fig. 3. Relative angle distributions for particles subject to confining potentials. For each model, different panels represent different degrees of temporal coarse-graining as indicated. (*A*) Diffusion in a square box. The trajectory was obtained by integrating Eq. **3** with $m = 1$ and $\sqrt{\mathcal{D}}/\gamma = 0.1$ in a 10×10 region; the time step and sampling interval were both 0.1. (*B*) Dynamics steered by a harmonic potential. Same parameters as in *A* with a similar effective bounding region: $\langle(x - \langle x\rangle)^2\rangle = \langle(y - \langle y\rangle)^2\rangle = 25/3$ and drift $\langle x(t)\rangle = \langle y(t)\rangle = 0.003t$.

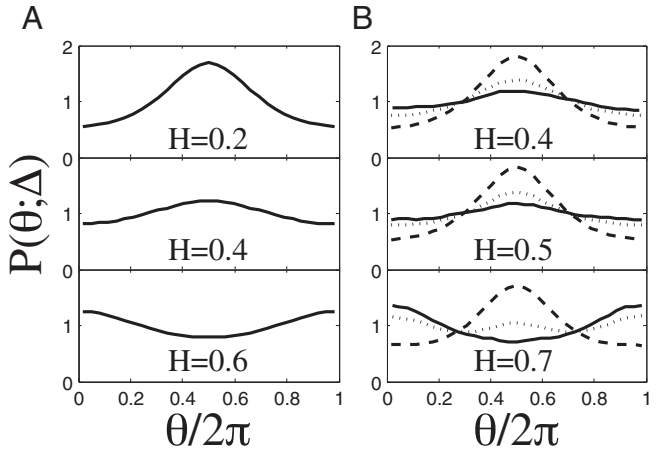

Fig. 4. Relative angle distributions for random walks leading to anomalous (non-Brownian) dynamics. Different panels correspond to different parameter choices. (*A*) Fractional Brownian motion (FBM). Panels show $\Delta = 100$ behavior for different Hurst exponents as indicated. We use the method of ref. 36 to produce FBM with an average step length of 1; 1,000 different trajectories were produced with 10,000 steps each. (*B*) Introduction of a power-law dwell time distribution. A random walk with FBM subordinated to a continuous time random walk (CTRW) with $H = 0.2$, $H = 0.5$, and $H = 0.7$. The $H = 0.5$ case is equivalent to a pure CTRW. For all H values, the different line types correspond to different temporal coarse-grainings: $\Delta = 100$ (dashed), $\Delta = 10{,}000$ (dotted) and $\Delta = 30{,}000$ (solid). The trajectories were produced by first generating FBM sequences similar to *A* and then inserting between every two steps dwell times τ that were generated with distribution $\psi(\tau) \sim \tau^{-1.8}$ for $\tau > 1$. During the τ periods, the dynamics of the particle follow Eq. **3** with $m = 1$, $\gamma = 1$, $\mathcal{D} = 0.6$, time step 0.1, and an additional force $-0.2(\mathbf{X}(t) - \mathbf{X}_s)$, where $\mathbf{X}_s$ is the starting position of the dwell period. At the end of time interval τ, the particle makes a jump according to the FBM sequence.

the distribution converges to a stationary profile, again characteristic of a self-similarity. Analogous behavior is observed for other confining potentials, with the shape of the peak at $\theta = \pi$ dependent on the details of the specific form.

In Fig. 3*B*, we show the behavior of $P(\theta;\Delta)$ of a particle under the influence of a harmonic potential with a steadily translating minimum (i.e., a steered dynamics, as in an optical trap experiment). At finite times, the distribution is peaked at $\theta = \pi$ due to the trap, just like the situation immediately above. However, as the confining potential moves, the particle dynamics are positively correlated overall, causing the peak to break in two and ultimately give rise to an inertial signature (compare Fig. 3*B*, Δ = 24000, with Fig. 2, Δ = 1).

Complex media can give rise to more complex dynamics with correlated steps, as discussed in the Introduction. For example, transport in a viscoelastic environment is expected to give rise to FBM (19). FBM is a stationary Gaussian process where the spatial position $X(t)$ is correlated such that $\langle X(t)X(t+\Delta)\rangle \sim \left(|t|^{2H} + |t+\Delta|^{2H} - |\Delta|^{2H}\right)$, where H is the Hurst exponent. When $0 < H < 1/2$, the motion is subdiffusive because the steps are negatively correlated, and we find $P(\theta;\Delta)$ to be akin to that of a confining potential (Fig. 4*A*; $H = 0.2$ and 0.4)—i.e., there is a tendency for reversals. In contrast, when $1/2 < H < 1$, the motion is superdiffusive because the steps are positively correlated and we find an interial-like signature (Fig. 4*A*; $H = 0.6$).

As already discussed, alternative anomalous dynamics arise from a power-law distribution of dwell times for steps (i.e., a CTRW). A pure CTRW signature is shown in Fig. 4*B* ($H = 0.5$). The directional anticorrelation peak at $\theta = \pi$ decreases with Δ. When the step sizes are described by FBM and the dwell times are described by CTRW (i.e., when ergodic and nonergodic processes coexist), we say that FBM is subordinated to CTRW (see refs. 4, 15, and 20 for examples). Examples of $P(\theta;\Delta)$ for such dynamics are shown in the remaining panels in Fig. 4*B*. The $H = 0.2$ case is quite similar to the CTRW (H = 0.5), but, in the $H = 0.7$ case (i.e., when there are positively correlated steps, as in the case of active transport), there is a progression from a confined signature to an inertial one with increasing temporal coarse-graining. However, note that, in contrast to Fig. 3*B*, the peak at $\theta = 0$ emerges without the peak at $\theta = \pi$ splitting. In other words, the qualitative shape of the profiles at intermediate values of Δ can be used to distinguish different motions.

Application to Experimental Data

We examine $P(\theta;\Delta)$ for particle tracking data from three different experimental situations.

Colloidal Suspensions. The first system is driven only by thermal energy. It is a colloidal suspension of 1.58 ± 0.04-μm-diameter silica spheres in water between parallel glass plates that are separated by 1.76 ± 0.05 μm (21). The data are those for packing fractions of $\phi = 0.316$ and $\phi = 0.681$ from ref. 21. We expect the colloidal particles to move freely at the former ϕ and to be close to jammed at the latter ϕ. Consistent with these ideas, we find that $P(\theta;\Delta)$ for $\phi = 0.316$ is almost flat (Fig. 5*B*, *Upper*), whereas that for $\phi = 0.681$ exhibits a pronounced peak at $\theta = \pi$ (Fig. 5*B*, *Lower*), similar to the profile for a particle in a box (Fig. 3*A*). The peak in Fig. 5*B*, *Lower* decays slightly as the temporal coarse-graining interval is lengthened; we interpret this decay to reflect the fact that particles are not completely confined by their neighbors—they eventually escape their neighbors and the system mixes after many such events. The dependence on Δ provides quantitative information about the time scale of such dynamics. Caging and escape were identified previously in colloidal suspensions (21, 22) and can be directly observed for specific trajectories. Likewise, backscattering of neighboring particles in simulations has long been visualized through the velocity autocorrelation function (23). However, $P(\theta;\Delta)$ provides a much more sensitive statistical probe: $P(\theta;\Delta)$ for $\phi = 0.68$ shows a peak at $\theta = \pi$ when the corresponding MSD is already linear (Fig. 5*A*).

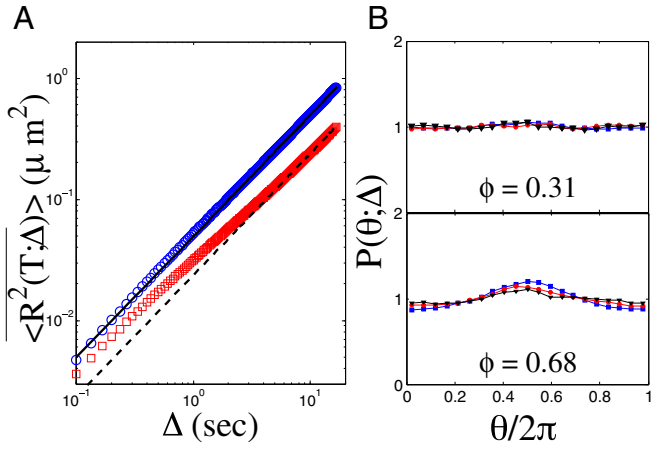

Fig. 5. Caging and escape in quasi-2D colloidal suspensions. (*A*) MSD for packing fractions $\phi = 0.31$ (blue circles) and $\phi = 0.68$ (red squares). The full black line (MSD = 1.73*s*) fits the $\phi = 0.31$ data at all times, whereas for the $\phi = 0.68$ case, a transition to linear behavior, black dashed line (MSD = 0.83*s*), occurs after about 2 s. (*B*) Relative angle distributions for $\phi = 0.31$ (*Upper*) and $\phi = 0.68$ (*Lower*). The curves correspond to temporal coarse-grainings of $\Delta = 50$ frames (blue squares), $\Delta = 150$ frames (red circles), and $\Delta = 250$ frames (black triangles) in both cases. Data are from ref. 21; the total measurement time in both cases is 33.3 s, with a frame rate of 30 Hz.

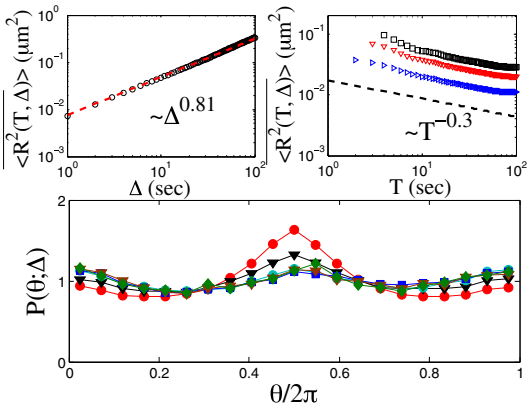

Fig. 6. Statistical measures of insulin granule transport in a pancreatic cell line (MIN6). (*Upper*) MSD as a function of lag time (*Left*) and measurement time (*Right*) for three constant Δ values: Δ = 1 s (blue), Δ = 2 s (red), and Δ = 3 s (black). (*Lower*) $P(\theta;\Delta)$ profiles for Δ = 1 frame (red), Δ = 5 frames (black), Δ = 10 frames (cyan), Δ = 20 frames (blue), Δ = 40 frames (brown), and Δ = 50 frames (green). MIN6 cells were cultured and imaged in DMEM at 37 °C under 5% (vol/vol) CO_2 gas. MIN6 cells were transfected with proinsulin-GFP (24) using Lipofectamine 2000 (Life Technologies 11668) with the manufacturer's recommended conditions. Imaging was done on a spinning-disk confocal microscope (3I Marianas system) with a 100×, 1.45 NA objective (alpha Plan-Fluar; Zeiss 421190–9900-000), at 1 Hz. Particle tracking was done with Diatrack 3.03 (Semasopht).

Insulin Granules. More complex dynamics can arise in systems with active elements, such as molecular motors. Here, we study the transport of insulin-containing vesicles (granules). In addition to active elements, these dynamics are influenced by fluctuations of the crowded cellular environment. Analysis of the MSD recently indicated that these granules combine ergodic and nonergodic random walk processes (4), and we showed that a hybrid model that subordinated a FBM with $H \approx 0.35$ to a CTRW with dwell time distribution $\psi(\tau) \sim \tau^{-(1+\beta)}$ (with $\beta \sim 0.8$) accounted for a host of statistics of the motion (4). This model provides a simple physical mechanism for obtaining characteristic insulin secretion profiles comprised of a burst followed by sustained release (see ref. 4 for further discussion of the biological implications). In the present study, we obtain similar scalings with different fluorescent constructs [proinsulin-enhanced green fluorescent protein (EGFP) (24) vs. syncollin-EGFP (4)]. Specifically, the dwell-time distribution exponent β is obtained from $\left\langle \overline{\mathbf{R}^2(T,\Delta)} \right\rangle \sim T^{\beta-1}$ (Fig. 6, *Upper Right*) (13) and then the Hurst exponent H is obtained from $\left| \overline{\mathbf{R}^2(T,\Delta)} \right| \sim \Delta^{\alpha}$ (Fig. 6, *Upper Left*) and $\alpha = 1 - \beta + 2H\beta$ (25).

We plot $P(\theta;\Delta)$ for various temporal coarse-grainings in Fig. 6. At small Δ, there are two peaks: a larger one at $\theta = \pi$ and a smaller one at $\theta = 0$. The former shrinks and the latter grows with Δ, ultimately becoming equal in size. Given the model in ref. 4, it is worth comparing the profile in Fig. 6 with those in Fig. 4. As discussed above, CTRW gives rise to an effective confinement, leading to a peak at $\theta = \pi$ (Fig. 4*B*), which decays to a uniform distribution of θ as particles escape their traps, in analogy to the colloidal suspension discussed above. The profile for FBM depends on the Hurst exponent. FBM with $H < 0.5$ (subdiffusive or negatively correlated steps) exhibits a peak at $\theta = \pi$ (Fig. 4*A*), whereas FBM with $H > 0.5$ (superdiffusive or positively correlated steps) exhibits a peak at $\theta = 0$. The subordinated model in ref. 4 combines CTRW with FBM with $H < 0.5$ and thus captures the peak at $\theta = \pi$, including its decay. However, that model fails to reproduce the peak at $\theta = 0$ that is characteristic of active transport. This limitation of the simple model in ref. 4 is not surprising, as a minority of the granules are superdiffusive (4).

We can reproduce the observed behavior (Fig. 7*A*, *Upper*) by expansion of the subordinated model to include Hurst exponents above and below 0.5 for different particles (Fig. 7*A*, *Lower*), as could arise from spatial heterogeneity within the cells. The main limitation of this approach is that $P(\theta;\Delta)$ is very sensitive to the distribution of H; the amplitude of the variation in $P(\theta;\Delta)$ is also restricted to the range shown. An alternative way to account for the observed shape of $P(\theta;\Delta)$ is to assume that the motion is anisotropic, again from spatial heterogeneity. We show the behavior for regular diffusion with two different ratios of diffusion coefficients in the Cartesian directions x and y in Fig. 7*B*. In this case, the profile can be tuned to make the peaks more pronounced. We do not detect global differences in properties of the motion, but it is possible for local differences to exist. A deeper understanding of the structure of $P(\theta;\Delta)$ for this system requires exploration of microscopic models with explicit molecular features, which is beyond the scope of the present study. Rather, the key point is that the relative angle distribution reveals directional correlations and self-similarity that are not evident in the MSD (or measures of angular correlation that are averages) (16), and these features can be used to further constrain models of transport.

Reconstituted Filament-Motor System. The final system that we consider comprises a mixture of filamentous actin (F-actin), myosin thick filaments (motors), and α-actinin (passive) cross-linkers on a model membrane substrate. This system with motor densities ≥0.3 μm^{-2} was used recently to show that F-actin buckling breaks the symmetry between extensile and compressive forces to generate contractility in cytoskeletal networks lacking sarcomeric organization (26), as suggested previously (27, 28). Here, we study the motion of the motors when they are at a lower density (0.04 μm^{-2}) such that they do not perturb the F-actin structure.

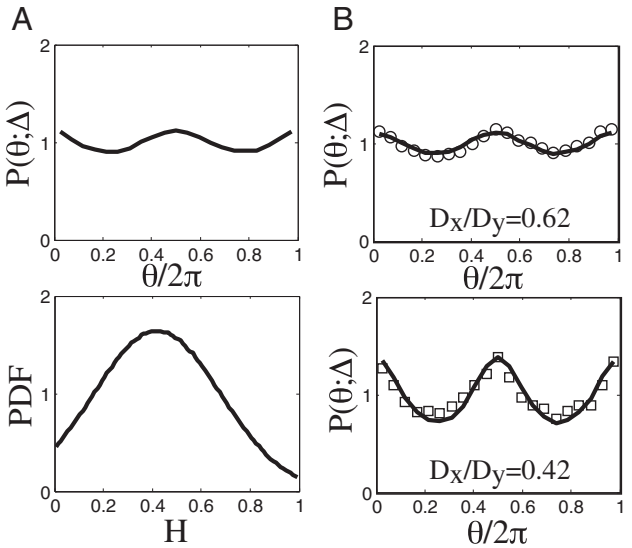

Fig. 7. Models that lead to stable $P(\theta;\Delta)$ profiles with peaks at $\theta = 0$ and $\theta = \pi$. (*A*) $P(\theta;\Delta)$ profile (*Upper*) obtained for an ensemble of trajectories in which each is generated by FBM with a randomly selected Hurst exponent, H. The H values are drawn from a Gaussian distribution with mean 0.42 and SD 0.26 that is truncated outside $0 < H < 1$ (*Lower*). (*B*) $P(\theta;\Delta)$ profiles for anisotropic diffusion with ratio $D_x/D_y = 0.62$ (*Upper*) and $D_x/D_y = 0.42$ (*Lower*). The symbols are experimental data: insulin granules with Δ = 20 (circles in upper panel) and myosin thick filaments with Δ = 20 (squares in lower panel).

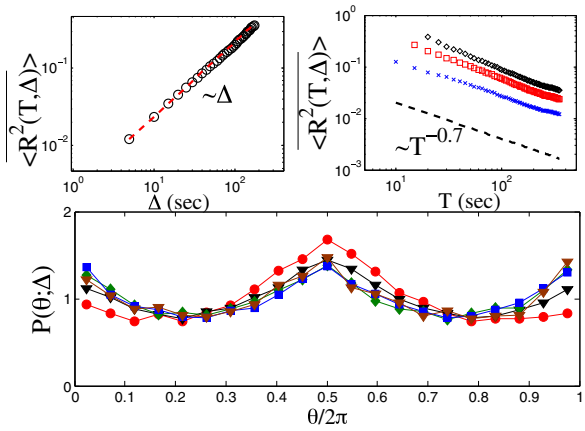

Fig. 8. Statistical measures of the motion of myosin thick filaments on a disordered actin network. (*Upper*) MSD as a function of lag time (*Left*) and measurement time (*Right*) for three constant Δ values: Δ = 5 s (blue), s (red), and Δ = 15 s (black). (*Lower*) $P(\theta;\Delta)$ profiles for Δ = 1 frame (red), Δ = 3 frames (black), Δ = 10 frames (green), Δ = 20 frames (blue), and Δ = 30 frames (brown). The frame rate is 5 Hz.

In contrast to the cellular system discussed above (4), the MSD varies linearly with lag time for this system (Fig. 8, *Upper Left*). The MSD thus suggests that the dynamics of this system are simpler than those of the insulin granules. However, the MSD decays with measurement time with power-law scaling (Fig. 8, *Upper Right*), as in the data for the insulin granules. We interpret this aging as evidence for local trapping. This picture and, more precisely, the MSD statistics are consistent with pure CTRW motion and glassy dynamics.

Nevertheless, $P(\theta;\Delta)$ for the actomyosin system resembles that for the pancreatic cell line, including the dependence on the temporal coarse-graining interval (Fig. 8, *Lower*). Again, this profile can be fit by a model with anisotropic diffusion, and the amplitudes of the peaks sets the difference in diffusion coefficient (here, $D_x/D_y = 0.42$; cf. Fig. 7*B*). This system thus provides an opportunity for investigating the directional correlations in a context in which all of the contributing elements are known. One possible scenario is that the heads of each myosin thick filament bind to different actin filaments and undergo a "tug-of-war" that ultimately gives way to movement in one direction. However, the fact that the peak at $\theta = 0$ does not grow without bound indicates that the directed motion cannot be sustained. The stationarity of the distribution (within experimentally accessible time scales) imposes strong restrictions on the microscopic dynamics and the structure of the filament network. Our goal is not to investigate these dynamics here. Rather, it is to show that the relative angle analysis reveals common features of the filament-motor dynamics (Figs. 6 and 8), in contrast to the MSD, which shows very different behaviors for the two systems (diffusive vs. subdiffusive scaling).

Conclusions

We have introduced an order parameter for quantifying directional motion in stochastic trajectories, the distribution of relative angles for different temporal coarse-grainings, $P(\theta;\Delta)$, and we have shown that it gives unique insights into particle tracking data. There is a long history of methods that seek to go beyond the MSD to characterize dynamics (29, 30), particularly since the advent of single-molecule tracking experiments. Recent innovations include comparing exchange and persistence time distributions to detect glassy behavior (31), *p*-variation (32), the mean maximal excursion method for anomalous diffusion (33), and the diffusivity distribution (34). However, these methods focus on distributions of extents of changes (e.g., distances traveled) and their scaling with time. By contrast, $P(\theta;\Delta)$ takes advantage of the fact that multidimensional measurements contain additional information about direction of motion. We find this order parameter to be a very sensitive measure of changes in dynamics, and it provides quantitative information about the time scales over which different dynamics contribute. These features are illustrated by our analysis of colloidal suspensions: $P(\theta;\Delta)$ clearly shows the transition from unconfined to confined dynamics with packing fraction, and it yields insights into the time scales for particles to escape their neighbors and mix. One recent study of lipid droplets in live cells did examine direction of motion but characterized it through the time correlation function for relative angles (16), which is an ensemble average. Although it has been shown that the velocity autocorrelation can yield information about subtle features, such as anharmonicity (30), in general, averaging obscures the heterogeneity in a population and the self-similarity of the motion. Our single-particle analysis here reveals such features in the filament-motor dynamics considered and thus provides constraints for the design of microscopic models of these systems. As 3D data become available, additional (dihedral) angles can be studied. Beyond that, an outstanding challenge is development of a theoretical framework for the order parameter and its behavior.

ACKNOWLEDGMENTS. We thank Monika Kauer for helpful discussions and a critical reading of the manuscript. This work was supported by the WM Keck Foundation, Novo Nordisk, National Science Foundation (NSF) Division of Materials Research (DMR) Materials Research Science and Engineering Center (MRSEC) Grant 0820054, and National Institutes of Health (NIH) R01-DK092616 and P30-DK020595. S.B. wishes to acknowledge the hospitality of the Aspen Center for Physics, which is partially supported by NSF Division of Physics (PHY) Grant 1066293.

1. Stefani FD, Hoogenboom JP, Barkai E (2009) Beyond quantum jumps: Blinking nanoscale light emitters. *Phys Today* 62:34.
2. Wang B, Anthony SM, Bae SC, Granick S (2009) Anomalous yet Brownian. *Proc Natl Acad Sci USA* 106(36):15160–15164.
3. Golding I, Cox EC (2006) Physical nature of bacterial cytoplasm. *Phys Rev Lett* 96(9): 098102.
4. Tabei SM, et al. (2013) Intracellular transport of insulin granules is a subordinated random walk. *Proc Natl Acad Sci USA* 110(13):4911–4916.
5. Sims DW, et al. (2008) Scaling laws of marine predator search behaviour. *Nature* 451(7182):1098–1102.
6. Viswanathan G, et al. (1996) Lévy flight search patterns of wandering albatrosses. *Nature* 381(6581):413–415.
7. Ramos-Fernadez G, et al. (2004) Lévy walk patterns in the foraging movements of spider monkeys (ateles geoffroyi). *Behav Ecol Sociobiol* 55(3):223–230.
8. Song C, Qu Z, Blumm N, Barabási AL (2010) Limits of predictability in human mobility. *Science* 327(5968):1018–1021.
9. Einstein A (1905) On the movement of small particles suspended in stationary liquids required by the molecular-kinetic theory of heat. *Ann Physik* 17(8):549–560.
10. Mandelbrot B, Ness JV (1968) Fractional Brownian motions, fractional noises and applications. *SIAM Rev* 10(4):422–437.
11. Deng W, Barkai E (2009) Ergodic properties of fractional Brownian-Langevin motion. *Phys Rev E Stat Nonlin Soft Matter Phys* 79(1 Pt 1):011112.
12. Montroll EW, Weiss GH (1965) Random walks on lattices. II. *J Math Phys* 6(2):167–181.
13. He Y, Burov S, Metzler R, Barkai E (2008) Random time-scale invariant diffusion and transport coefficients. *Phys Rev Lett* 101(5):058101.
14. Bel G, Barkai E (2005) Weak ergodicity breaking in the continuous-time random walk. *Phys Rev Lett* 94(24):240602.
15. Weigel AV, Simon B, Tamkun MM, Krapf D (2011) Ergodic and nonergodic processes coexist in the plasma membrane as observed by single-molecule tracking. *Proc Natl Acad Sci USA* 108(16):6438–6443.
16. Harrison AW, Kenwright DA, Waigh TA, Woodman PG, Allan VJ (2013) Modes of correlated angular motion in live cells across three distinct time scales. *Phys Biol* 10(3): 036002.
17. Kubo R, Toda N, Hashitsume N (1991) *Statistical Physics II* (Springer Verlag, Heidelberg).
18. Stanely HE (1996) *Fractals and Disordered Systems*, eds Bunde A, Havlin S (Springer Verlag, Heidelberg), p 1.
19. Goychuk I (2012) Viscoelastic subdiffusion: Generalized langevin equation approach. *Adv Chem Phys* 150:187–253.
20. Fogedby HC (1994) Langevin equations for continuous time Lévy flights. *Phys Rev E Stat Phys Plasmas Fluids Relat Interdiscip Topics* 50(2):1657–1660.

21. Cui B, Diamant H, Lin B, Rice SA (2004) Anomalous hydrodynamic interaction in a quasi-two-dimensional suspension. *Phys Rev Lett* 92(25 Pt 1):258301.
22. Weeks ER, Crocker JC, Levitt AC, Schofield A, Weitz DA (2000) Three-dimensional direct imaging of structural relaxation near the colloidal glass transition. *Science* 287(5453):627–631.
23. Alder BJ, Wainwright TE (1967) Velocity autocorrelations for hard spheres. *Phys Rev Lett* 18(23):988–990.
24. Rajan S, et al. (2010) In vitro processing and secretion of mutant insulin proteins that cause permanent neonatal diabetes. *Am J Physiol Endocrinol Metab* 298(3): E403–E410.
25. Meroz Y, Sokolov IM, Klafter J (2010) Subdiffusion of mixed origins: When ergodicity and nonergodicity coexist. *Phys Rev E Stat Nonlin Soft Matter Phys* 81(1 Pt 1):010101.
26. Murrell MP, Gardel ML (2012) F-actin buckling coordinates contractility and severing in a biomimetic actomyosin cortex. *Proc Natl Acad Sci USA* 109(51):20820–20825.
27. Lenz M, Thoresen T, Gardel ML, Dinner AR (2012) Contractile units in disordered actomyosin bundles arise from F-actin buckling. *Phys Rev Lett* 108(23):238107.
28. Lenz M, Gardel ML, Dinner AR (2012) Requirements for contractility in disordered cytoskeletal bundles. *New J Phys* 14:033037.
29. van Hove L (1954) Correlations in space and time and Born approximation scattering in systems of interacting particles. *Phys Rev* 95(1):249–262.
30. Grest GS, Nagel SR, Rahman A, Witten TA (1981) Density of states and the velocity autocorrelation function derived from quench studies. *J Chem Phys* 74(6):3532–3534.
31. Hedges LO, Maibaum L, Chandler D, Garrahan JP (2007) Decoupling of exchange and persistence times in atomistic models of glass formers. *J Chem Phys* 127(21):211101.
32. Magdziarz M, Weron A, Burnecki K, Klafter J (2009) Fractional Brownian motion versus the continuous-time random walk: A simple test for subdiffusive dynamics. *Phys Rev Lett* 103(18):180602.
33. Tejedor V, et al. (2010) Quantitative analysis of single particle trajectories: Mean maximal excursion method. *Biophys J* 98(7):1364–1372.
34. Wang B, Kuo J, Bae SC, Granick S (2012) When Brownian diffusion is not Gaussian. *Nat Mater* 11(6):481–485.
35. Burrage K, Lenane I, Lythe G (2007) Numerical methods for second-order stochastic differential equations. *SIAM J Sci Comput* 29:245–264.
36. Hosking JRM (1984) Modeling persistence in hydrological time series using fractional differencing. *Water Resour Res* 20(12):1898–1908.